

Oceanic detachment faults generate compression in extension

R. Parnell-Turner¹, R.A. Sohn¹, C. Peirce², T.J. Reston³, C.J. MacLeod⁴, R.C. Searle², and N.M. Simão².

¹Department of Geology and Geophysics, Woods Hole Oceanographic Institution, Woods Hole, Massachusetts 02543, USA

²Department of Earth Sciences, Durham University, South Road, Durham DH1 3LE, UK

³School of Geography, Earth and Environmental Sciences, University of Birmingham, Birmingham B15 2TT, UK

⁴School of Earth and Ocean Sciences, Cardiff University, Main Building, Park Place, Cardiff CF10 3AT, UK

ABSTRACT

In extensional geologic systems such as mid-ocean ridges, deformation is typically accommodated by slip on normal faults, where material is pulled apart under tension and stress is released by rupture during earthquakes and magmatic accretion. However, at slowly spreading mid-ocean ridges where the tectonic plates move apart at rates <80 km m.y.⁻¹, these normal faults may roll over to form long-lived, low-angled detachments that exhume mantle rocks and form corrugated domes on the seabed. Here we present the results of a local micro-earthquake study over an active detachment at 13°20'N on the Mid-Atlantic Ridge to show that these features can give rise to reverse-faulting earthquakes in response to plate bending. During a 6 month survey period, we observed a remarkably high rate of seismic activity, with $>244,000$ events detected along 25 km of the ridge axis, to depths of ~ 10 km below seafloor. Surprisingly, the majority of these were reverse-faulting events. Restricted to depths of 3–7 km below seafloor, these reverse events delineate a band of intense compressional seismicity located adjacent to a zone of deeper extensional events. This deformation pattern is consistent with flexural models of plate bending during lithospheric accretion. Our results indicate that the lower portion of the detachment footwall experiences compressive stresses and deforms internally as the fault rolls over to low angles before emerging at the seafloor. These compressive stresses trigger reverse faulting even though the detachment itself is an extensional system.

INTRODUCTION

Oceanic lithosphere is formed at mid-ocean ridges by a combination of magmatism and normal faulting, driven by far-field forces arising from processes including plate subduction and mantle convection (Lachenbruch, 1976). In these extensional settings, a portion of the strain is expected to be accommodated by slip on normal faults, which is reflected in the focal mechanisms of earthquakes observed near the spreading axis (Sykes, 1967). At slow-spreading ridges, accounting for large parts of the lithosphere accreted in the Atlantic, Indian, and Arctic Oceans, young lithosphere may be deformed by slip along large-offset normal faults called detachments (Cann et al., 1997; Tucholke et al., 1998; Dick et al., 2003; Escartín et al., 2008b). Detachment faults can exhume lower crustal gabbros and serpentinized mantle peridotites at the seabed and form kilometer-scale dome-shaped features called oceanic core complexes (Cann et al., 1997; MacLeod et al., 2002; Escartín et al., 2003; Grimes et al., 2008). The mechanical behavior of detachment faults is controversial because the domed fault surfaces emerge from the seafloor at low angles that are incompatible with the physics of extensional faulting (Buck et al., 2005). There is evidence for fault initiation on a steeply dipping, deeply penetrating rupture

surface (MacLeod et al., 2009, 2011; Morris et al., 2009), but the mechanism by which the fault rolls over to low angles prior to seafloor exhumation is poorly understood. Local earthquake surveys with ocean bottom seismographs (OBSs) have the potential to address this issue; however, previous OBS deployments at oceanic detachments had insufficient aperture and instrument density to resolve the mechanics of fault rollover (deMartin et al., 2007; Collins et al., 2012; Grevenmeyer et al., 2013). Intriguingly, a few reverse-faulting events were observed beneath the Logatchev core complex on the Mid-Atlantic Ridge at 14°40'N, but the relationship of these events to the extensional fault system was unclear, and they were attributed to volume expansion from serpentinization or magma-chamber filling rather than deformation on a detachment fault (Grevenmeyer et al., 2013).

MICRO-EARTHQUAKE EXPERIMENT

In 2014, we conducted the largest micro-earthquake experiment to date at a slow-spreading ridge. A dense network of 25 short-period OBSs (instrument spacing of 2–3 km) was deployed for a 6 month period along ~ 10 km of the ridge axis at 13°N on the Mid-Atlantic Ridge (Fig. 1). Detachment faults are common in this region, including two well-surveyed

and sampled oceanic core complexes located at 13°20'N and 13°30'N (Smith et al., 2006; MacLeod et al., 2009; Mallows and Searle, 2012; Escartín et al., 2017). Both core complexes have well-developed, domed, corrugated surfaces and are accompanied by a high level of hydroacoustically recorded seismicity, suggesting that they are currently active or have been in the recent geological past (Smith et al., 2008; MacLeod et al., 2009; Mallows and Searle, 2012).

We recorded $>244,000$ events on more than three stations during the 198-day deployment, yielding a mean rate of ~ 1240 micro-earthquakes per day (see Methods in the GSA Data Repository¹), two orders of magnitude greater than that observed at the Logatchev core complex (Grevenmeyer et al., 2013). This remarkably high rate of seismicity was fairly constant throughout the deployment period (Fig. 2B). There was no evidence for foreshock–main shock sequences, except for a small seismic swarm in the western band of events at Julian day 280 within a region extending 3 km south from the northern tip of the band. The locations and focal mechanisms of these events are indistinguishable from the rest of the seismicity in this area. Events have small local magnitude (M_L), ranging between -1.0 and 2.7 and with a modal average of 0.3 (Fig. DR1 in the Data Repository). The high number of earthquakes, combined with the dense seismic network, allowed us to estimate hypocenters and focal mechanism solutions for a subset of 18,313 well-characterized events (see the Data Repository). These reveal that reverse faulting was the most common mode of deformation near the 13°20'N detachment during our deployment (Fig. 1). The compressional events define a distinct arc of intense seismicity that wraps around the detachment trace (on the eastern edge of the corrugated surface), at depths of 3–7 km beneath the seabed (Fig. 2; Fig. DR2). The slip directions (i.e., rake) of these events are typical of reverse and

¹GSA Data Repository item 2017309, additional information and figures describing the acquisition and processing of the microearthquake data set, and details of the elastic-plastic model, is available online at <http://www.geosociety.org/datarepository/2017/> or on request from editing@geosociety.org.

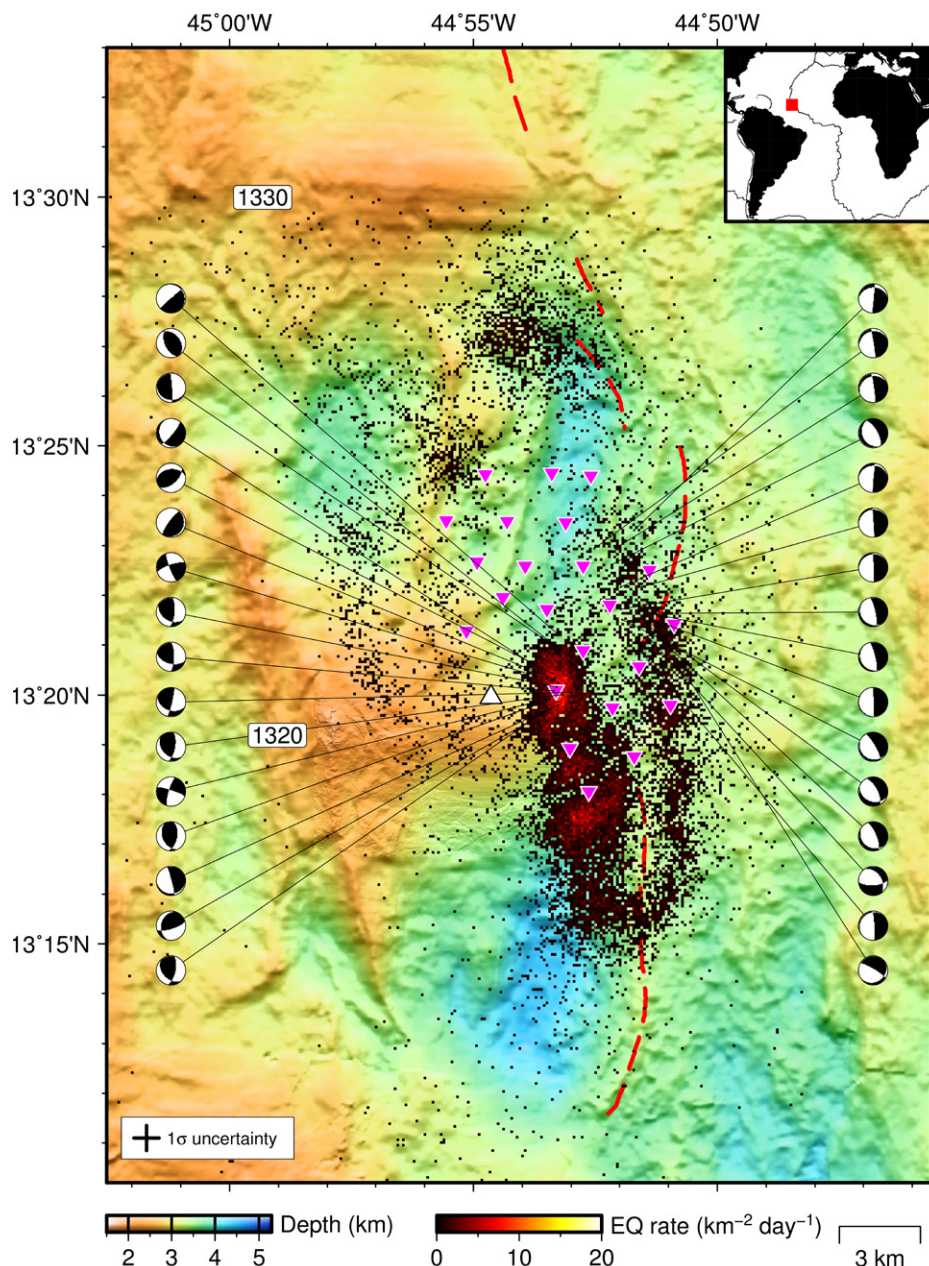


Figure 1. Bathymetric map with seismicity and focal mechanisms at 13°20'N on Mid-Atlantic Ridge (MAR). Inset shows location of study site (red box) and mid-ocean ridges (black lines). Main panel shows seismicity rate (EQ rate) calculated in 100 × 100 m bins for 18,313 well-constrained, relocated events, each detected by more than nine instruments. Randomly selected first-motion focal mechanism solutions are plotted in lower-hemisphere projection; red line shows neovolcanic zone; pink triangles show ocean-bottom seismograph positions; white triangle is Irinovskoe vent field. Location of along-axis adjacent corrugated oceanic core complexes is shown by 1320 and 1330 labels. Cross shows average 68% confidence level horizontal location uncertainty (0.9 km).

reverse-oblique faults. The compression (*P*) axes are dominantly subhorizontal, but there is no preferred orientation for the dip and strike of the fault planes (Fig. 2C). Events within the reverse-faulting band of seismicity have slightly smaller magnitudes than those in the normal-faulting band (Fig. DR1). In contrast, normal faulting is restricted to a narrow band of seismicity ~3 km east of the reverse-faulting zone, at depths of 7–12 km beneath the seabed (Fig. 2; Fig. DR2).

These event depths, which are comparable to the depth of normal-faulting seismicity observed at the Trans-Atlantic Geotraverse (TAG) detachment (deMartin et al., 2007), clearly show that extensional faulting extends beneath the crust. Focal mechanisms indicate steeply dipping (50°–70°) normal faults oriented subparallel to the near-north-south-trending spreading axis (Mallows and Searle, 2012) (Fig. 2C), and tension (*T*) axes indicating consistent extensional

stress oriented parallel to the spreading direction (~273°).

DISCUSSION

Our observations indicate that lithospheric extension at the 13°20'N detachment generates both compressional and extensional seismicity contemporaneously. The band of intense reverse faulting at 3–7 km depth is located directly beneath the hanging-wall cutoff, where the gently dipping corrugated surface emerges on the seafloor (Fig. 2E), and hence cannot lie on the detachment fault plane itself. Instead, this reverse faulting must be occurring within the detachment footwall. An active high-temperature vent field is located on the 13°20'N corrugated surface (Escartín et al., 2017), which could indicate footwall emplacement of magma bodies (Fig. 1); however, the vent site is located 2.3 km west of the band of reverse faulting (Fig. 2E), and cooling of a magma body should generate tensile, rather than compressive, stresses. Thermal contraction associated with heat extraction from a footwall magma body is therefore not a plausible source mechanism for the shallow band of compressive seismicity. Our observations instead support a model in which internal deformation of the lithosphere in response to flexural bending stress results in a high level of seismicity at the point of maximum bending (Lavie et al., 1999; Buck et al., 2005). The variability in the strike and dip of fault-plane solutions (*P*- and *T*-axes) in this zone indicates distributed, isotropic deformation of the deeper, internal portion of the detachment footwall (Fig. 2C). In contrast, toward the center of the axial valley and at greater depth (6–10 km), steep, ridge-parallel normal faulting accommodates extensional deformation on the active detachment as new material accretes into the footwall. The short distance between bands of reverse and normal faulting (~2 km perpendicular to the fault plane) requires a rapid change in the footwall stress field over a short length-scale, from extensional stresses in the accretion zone to compressive stresses in the region of fault rollover. This observation, combined with the spatially restricted zone of reverse faulting, indicates that fault rollover may be a relatively abrupt, rather than gradual, process, with tightening of curvature at progressively shallower subsurface depths.

We have developed a simple model based upon the deflection of a bending plate with elastic-plastic rheology to reconcile our observations (see the Data Repository; McAdoo et al., 1978). The model is constrained by the location and dip of the corrugated fault surface at the seafloor, the spatial distribution and focal mechanisms of observed earthquakes, and a lithospheric slab thickness of 6 km inferred from the depth distribution of seismicity. We use the distribution of earthquakes in the footwall to

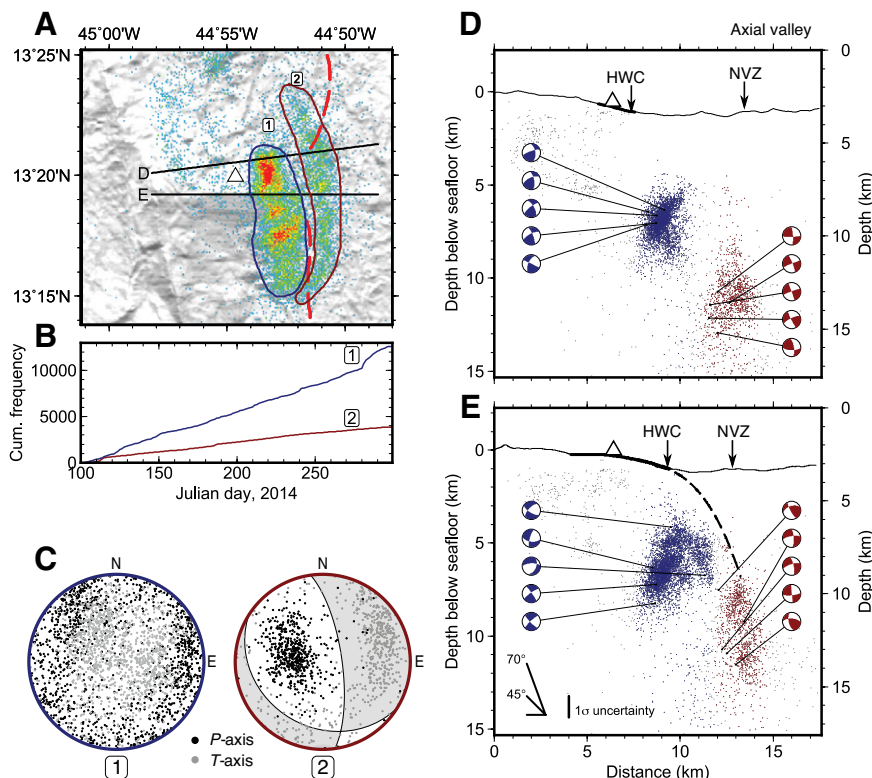


Figure 2. Seismicity rate and cross sections. **A:** Shaded-relief bathymetry (illuminated from northeast) with cumulative seismic moment release in dyn cm^{-1} ; red and blue polygons delineate domains shown in B and C; black lines are transects shown in D and E; white triangle is vent field; red line is neovolcanic zone (NVZ). **B:** Seismicity time series for domains 1 (blue) and 2 (red). Cum.—cumulative. **C:** Stereonets with *P*- (black) and *T*-axes (gray) for events in domains 1 and 2; gray shading is best-fitting fault plane solution for domain 2 (strike 352° and dip 72°E). **D, E:** Cross sections with hypocenters colored by domain as in A and representative focal mechanisms (cross sections through lower-hemisphere projection). Black solid line is seabed; thickened sections indicate corrugated fault scarp exposure; dashed line is calculated plate deflection from elastic-plastic model, applicable to spreading-parallel profile in E only; arrows show location of hanging-wall cutoff (HWC) and nearest along-strike projection of NVZ. Vertical bar shows average 68% confidence level vertical uncertainty (1.15 km).

define a stress profile, with “plastic” failure at depths where seismic events are observed (in elastic-plastic models, deformation from earthquakes is treated as bulk “plastic” yielding), and assume that the initiating fault is likely to have a maximum dip of $\sim 70^\circ$. We seek a bending profile that satisfies these constraints by varying the mechanical strength of the plate in terms of its flexural rigidity, or effective elastic thickness (T_e). We find that a best fit is obtained if T_e increases linearly from 0.7 km near the spreading axis to 0.9 km at the point where the footwall emerges at the seafloor (dashed line, Fig. 2E). This range in T_e , which is a modeling parameter rather than a physical property of the lithosphere, is consistent with previous estimates from bathymetric profiles of detachment-faulted terrain (Schouten et al., 2010). Our simple model demonstrates that the location of the reverse faulting is consistent with that predicted by bending of the detachment footwall under a mechanically reasonable deflection profile (Fig. 3). Reverse faulting is not observed at the TAG detachment (deMartin et al., 2007), which

is younger and less mature than the $13^\circ 20'\text{N}$ detachment. This lack of reverse faulting could be explained by a young system not having a sufficiently well-developed dome to produce compression in the footwall; however, without further observations at other young detachments, this suggestion remains speculative.

The two bands of seismicity show well-defined along-axis extents, the northern ends of which lie within the OBS network and are therefore well resolved. The extent of the western, compressional band roughly matches that of the corrugated surface between $13^\circ 15'$ and $13^\circ 21'\text{N}$, north of which the neovolcanic zone begins to develop (Fig. 1). The band of normal faulting extends ~ 3 km further north to $13^\circ 23'\text{N}$, beyond which the seismicity rate is remarkably low. These results demonstrate that the nature of seismically accommodated deformation changes significantly at the northern limit of the $13^\circ 20'\text{N}$ core complex, but the inability of our network to provide focal mechanism solutions in this area makes it difficult to interpret this change in the context of fault structure and deformation. A

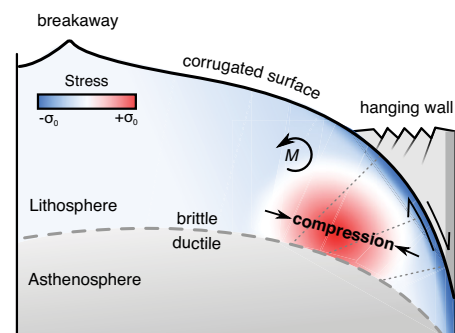


Figure 3. Schematic diagram of stress fields generated by deformation at mature oceanic detachment faults. Most of lithosphere is under tension, but bending (M) associated with fault rollover to low dip angles generates compressive stresses (red shading) in lower portion of fault footwall. Gray dotted lines are markers perpendicular to fault surface; gray dashed line shows nominal base of lithosphere; apparent deepening of brittle-ductile transition in common with Trans-Atlantic Geotraverse (TAG) (deMartin et al., 2007). Earthquakes are expected in zones where stress exceeds yield stress ($|\sigma| > |\sigma_0|$), consistent with our observations. Hanging wall is tectonized and thus weak, which facilitates penetration of seawater into upper part of fault zone.

swarm of 276 events occurred over a 3–4 day period at $13^\circ 27'\text{N}$, just south of the $13^\circ 30'\text{N}$ core complex, which is suggestive of magmatic activity; this interpretation, however, is necessarily tentative because we cannot obtain focal mechanism estimates from this area.

The apparent lack of seismicity on the upper surface of the detachment footwall at shallow crustal depths is enigmatic. Extensional bending stresses are clearly high in this region, and there must be slip between the footwall and hanging wall on the fault surface. Rock samples recovered from the $13^\circ 20'\text{N}$ detachment fault scarp are dominated by hydrothermal quartz-cemented basalt breccia, in addition to sheared serpentinites, talc schists, incohesive cataclases, and hydrothermal deposits (MacLeod et al., 2009; Escartín et al., 2014, 2017). This assemblage provides evidence for significant hydrothermal alteration and mineralization in the fault zone, which may modify the rheology of these rocks and preclude the generation of detectable seismicity (Reinen et al., 1992; Escartín et al., 2008a). Alternatively, we cannot rule out the possibility that deformation in this zone occurs episodically over time intervals that are long compared to the duration of our observations.

CONCLUSIONS

We find that accretion and extension of oceanic crust at the $13^\circ 20'\text{N}$ detachment is accommodated by two distinct modes of deformation, reflecting two stages of lithospheric evolution. First, extensional faulting occurs at the point where the detachment fault initiates at depths

of 6–10 km. These high-angle normal faults accommodate the far-field forces that drive plate separation as lower crustal and upper mantle rocks are incorporated into newly forming lithosphere in the rising fault footwall. **Second**, as the footwall rotates to lower angles, bending stresses lead to internal compression in the lower half of the plate. **As a result, reverse faults initiate within the bending lithosphere at depths of 3–7 km below where the footwall emerges at the seafloor to form a domed, corrugated fault surface** (Fig. 3). This evolution of footwall stress is consistent with kinematic models for detachment fault behavior (Buck, 1988) and with direct observations for reverse faulting in detachment fault footwalls (Pressling et al., 2012), suggesting that reverse faulting may be ubiquitous in mature, active oceanic detachments. **Our results provide a new framework for interpreting detachment seismicity and suggest that reverse-faulting events reported at other core complexes may have been triggered by bending stresses rather than volume expansion** (e.g., serpentinization). The mechanical regime we describe shows that **plate bending associated with the exhumation and formation of oceanic core complexes can generate compressional stresses leading to reverse faulting, despite being situated in an extensional stress regime.**

ACKNOWLEDGMENTS

This research was funded by Natural Environment Research Council (NERC) grants NE/J02029X/1, NE/J021741/1, and NE/J022551/1, and by U.S. National Science Foundation grant OCE-1458084. Instruments were provided by the NERC UK Ocean-Bottom Instrumentation Facility (Minshull et al., 2005). We are grateful to the officers, crew, technicians, and science parties of RRS *James Cook* cruises JC102, JC109, and JC132 for their hard work and professionalism. We thank V. Schlindwein and five anonymous reviewers for their constructive comments.

REFERENCES CITED

- Buck, W.R., 1988, Flexural rotation of normal faults: *Tectonics*, v. 7, p. 959–973, doi:10.1029/TC007i005p00959.
- Buck, W.R., Lavier, L., and Poliakov, A.N.B., 2005, Modes of faulting at mid-ocean ridges: *Nature*, v. 434, p. 719–723, doi:10.1038/nature03358.
- Cann, J.R., Blackman, D.K., Smith, D.K., McAllister, E., Janssen, B., Mello, S., Avgerinos, E., Pascoe, A.R., and Escartín, J., 1997, Corrugated slip surfaces formed at ridge-transform intersections on the Mid-Atlantic Ridge: *Nature*, v. 385, p. 329–332, doi:10.1038/385329a0.
- Collins, J.A., Smith, D.K., and McGuire, J.J., 2012, Seismicity of the Atlantis Massif detachment fault, 30°N at the Mid-Atlantic Ridge: *Geochemistry Geophysics Geosystems*, v. 13, Q0AG11, doi:10.1029/2012GC004210.
- deMartin, B.J., Sohn, R.A., Canales, J.P., and Humphris, S.E., 2007, Kinematics and geometry of active detachment faulting beneath the Trans-Atlantic Geotraverse (TAG) hydrothermal field on the: *Geology*, v. 35, p. 711–714, doi:10.1130/G23718A.1.
- Dick, H.J.B., Lin, J., and Schouten, H., 2003, An ultraslow-spreading class of ocean ridge: *Nature*, v. 426, p. 405–412, doi:10.1038/nature02128.
- Escartín, J., Mével, C., MacLeod, C.J., and McCaig, A.M., 2003, Constraints on deformation conditions and the origin of oceanic detachments: The Mid-Atlantic Ridge core complex at 15°45'N: *Geochemistry Geophysics Geosystems*, v. 4, 1067, doi:10.1029/2002GC000472.
- Escartín, J., Andreani, M., Hirth, G., and Evans, B., 2008a, Relationships between the microstructural evolution and the rheology of talc at elevated pressures and temperatures: *Earth and Planetary Science Letters*, v. 268, p. 463–475, doi:10.1016/j.epsl.2008.02.004.
- Escartín, J., Smith, D.K., Cann, J.R., Schouten, H., Langmuir, C.H., and Escrig, S., 2008b, Central role of detachment faults in accretion of slow-spreading oceanic lithosphere: *Nature*, v. 455, p. 790–794, doi:10.1038/nature07333.
- Escartín, J., et al., 2014, Insights into the internal structure and formation of striated fault surfaces of oceanic detachments from in situ observations (13°20'N and 13°30'N, Mid-Atlantic Ridge): Abstract T54A-01 presented at 2014 Fall Meeting, American Geophysical Union, San Francisco, California, 15–19 December.
- Escartín, J., et al., 2017, Tectonic structure, evolution, and the nature of oceanic core complexes and their detachment fault zones (13°20' N and 13°30'N, Mid Atlantic Ridge): *Geochemistry Geophysics Geosystems*, v. 18, p. 1451–1482, doi:10.1002/2016GC006775.
- Grevenmeyer, I., Reston, T.J., and Moeller, S., 2013, Microseismicity of the Mid-Atlantic Ridge at 7°S–8°15'S and at the Logatchev Massif oceanic core complex at 14°40'N–14°50'N: *Geochemistry Geophysics Geosystems*, v. 14, p. 3532–3554, doi:10.1002/ggge.20197.
- Grimes, C.B., John, B.E., Cheadle, M.J., and Wooden, J.L., 2008, Protracted construction of gabbroic crust at a slow spreading ridge: Constraints from ²⁰⁶Pb/²³⁸U zircon ages from Atlantis Massif and IODP Hole U1309D (30°N, MAR): *Geochemistry Geophysics Geosystems*, v. 9, Q08012, doi:10.1029/2008GC002063.
- Lachenbruch, A.H., 1976, Dynamics of a passive spreading center: *Journal of Geophysical Research*, v. 81, p. 1883–1902, doi:10.1029/JB081i011p01883.
- Lavier, L., Buck, W.R., and Poliakov, A., 1999, Self-consistent rolling-hinge model for the evolution of large-onset low-angle normal faults: *Geology*, v. 27, p. 1127–1130, doi:10.1130/0091-7613(1999)027<1127:SCRHMF>2.3.CO;2.
- MacLeod, C.J., et al., 2002, Direct geological evidence for oceanic detachment faulting: The Mid-Atlantic Ridge, 15°45'N: *Geology*, v. 30, p. 879–882, doi:10.1130/0091-7613(2002)030<0879:DGEFOD>2.0.CO;2.
- MacLeod, C.J., Searle, R.C., Murton, B.J., Casey, J.F., Mallows, C., Unsworth, S.C., Achenbach, K.L., and Harris, M., 2009, Life cycle of oceanic core complexes: *Earth and Planetary Science Letters*, v. 287, p. 333–344, doi:10.1016/j.epsl.2009.08.016.
- MacLeod, C.J., Carlut, J., Escartín, J., Horen, H., and Morris, A., 2011, Quantitative constraint on footwall rotations at the 15°45'N oceanic core complex, Mid-Atlantic Ridge: Implications for oceanic detachment fault processes: *Geochemistry Geophysics Geosystems*, v. 12, Q0AG03, doi:10.1029/2011GC003503.
- Mallows, C., and Searle, R.C., 2012, A geophysical study of oceanic core complexes and surrounding terrain, Mid-Atlantic Ridge 13°N–14°N: *Geochemistry Geophysics Geosystems*, v. 13, Q0AG08, doi:10.1029/2012GC004075.
- McAdoo, D.C., Caldwell, J.G., and Turcotte, D.L., 1978, On the elastic-perfectly plastic bending of the lithosphere under generalized loading with application to the Kuril Trench: *Geophysical Journal International*, v. 54, p. 11–26, doi:10.1111/j.1365-246X.1978.tb06753.x.
- Minshull, T.A., Sinha, M.C., and Peirce, C., 2005, Multi-disciplinary, sub-seabed geophysical imaging: *Sea Technology*, v. 46, no. 10, p. 27–31.
- Morris, A., Gee, J.S., Pressling, N., John, B.E., MacLeod, C.J., Grimes, C.B., and Searle, R.C., 2009, Footwall rotation in an oceanic core complex quantified using reoriented Integrated Ocean Drilling Program core samples: *Earth and Planetary Science Letters*, v. 287, p. 217–228, doi:10.1016/j.epsl.2009.08.007.
- Pressling, N., Morris, A., John, B.E., and MacLeod, C.J., 2012, The internal structure of an oceanic core complex: An integrated analysis of oriented borehole imagery from IODP Hole U1309D (Atlantis Massif): *Geochemistry Geophysics Geosystems*, v. 13, Q04G10, doi:10.1029/2012GC004061.
- Reinen, A., Tullis, E., and Weeks, D., 1992, Two-mechanism model for frictional sliding of serpentinite: *Geophysical Research Letters*, v. 19, p. 1535–1538, doi:10.1029/92GL01388.
- Schouten, H., Smith, D.K., Cann, J.R., and Escartín, J., 2010, Tectonic versus magmatic extension in the presence of core complexes at slow-spreading ridges from a visualization of faulted seafloor topography: *Geology*, v. 38, p. 615–618, doi:10.1130/G30803.1.
- Smith, D.K., Cann, J.R., and Escartín, J., 2006, Wide-spread active detachment faulting and core complex formation near 13°N on the Mid-Atlantic Ridge: *Nature*, v. 442, p. 440–443, doi:10.1038/nature04950.
- Smith, D.K., Escartín, J., Schouten, H., and Cann, J.R., 2008, Fault rotation and core complex formation: Significant processes in seafloor formation at slow-spreading mid-ocean ridges (Mid-Atlantic Ridge, 13°–15°N): *Geochemistry Geophysics Geosystems*, v. 9, Q03003, doi:10.1029/2007GC001699.
- Sykes, L.R., 1967, Mechanism of earthquakes and nature of faulting on the mid-oceanic ridges: *Journal of Geophysical Research*, v. 72, p. 2131–2153, doi:10.1029/JZ072i008p02131.
- Tucholke, B.E., Lin, J., and Kleinrock, M.C.C., 1998, Megamullions and mullion structure defining oceanic metamorphic core complexes on the Mid-Atlantic Ridge: *Journal of Geophysical Research*, v. 103, p. 9857–9866, doi:10.1029/98JB00167.

Manuscript received 21 February 2017
Revised manuscript received 13 April 2017
Manuscript accepted 19 June 2017

Printed in USA